

# New Frontier in Terahertz Technologies for Virus Sensing

Tiziana Mancini <sup>1</sup>, Augusto Marcelli <sup>2,3</sup>, Stefano Lupi <sup>1,4</sup> and Annalisa D'Arco <sup>1,2,\*</sup><sup>1</sup> Department of Physics, University of Rome 'La Sapienza', P.le A. Moro 2, 00185 Rome, Italy<sup>2</sup> Laboratori Nazionali Frascati, Istituto Nazionale di Fisica Nucleare, Via Enrico Fermi 54, 00044 Frascati, Italy<sup>3</sup> Rome International Centre for Materials Science Superstipes, Via dei Sabelli 119A, 00185 Rome, Italy<sup>4</sup> National Institute for Nuclear Physics Unit Rome1, P.le A. Moro 2, 00185 Rome, Italy

\* Correspondence: annalisa.darco@uniroma1.it

**Abstract:** The recent pandemic of SARS-CoV-2 virus has made evident critical issues relating to virus sensing and the need for deployable tools for adequate, rapid, effective viral recognition on a large-scale. Although many conventional molecular and immuno-based techniques are widely used for these purposes, they still have some drawbacks concerning sensitivity, safety, laboriousness, long-term collection and data analysis. Therefore, new rapidly emerging approaches have been introduced such as terahertz (THz)-based technologies. In this contribution, we summarize the emerging THz radiation technology, its solutions and applications for high-sensitivity viral detection.

**Keywords:** THz radiation; THz spectroscopy; THz technology; virus sensing; metamaterials; plasmonics; biosensing; surface plasmon resonance

## 1. Introduction

Pandemic crises, caused by infections due to Zika, Ebola, and the recent severe acute respiratory syndrome coronaviruses such as SARS-CoV-2, are burdening the healthcare systems, seriously threatening societal and economic stability [1]. Furthermore, the extent of the recent SARS-CoV-2 pandemic, its rapid large-scale spreading, the challenging management in many countries and the low reliability of early screening protocols have seriously impacted the healthcare systems. It is needless to say that effective virus diagnostic methods, based on rapid, reliable and accurate monitoring, can contribute toward controlling and preventing future pandemic events. Nowadays, the most widely used methods for viral diagnosis are mainly based on biomolecular techniques and immunoassays [2–8], namely, CRISPR–Cas12- [9] and CRISPR–Cas13-based SHERLOCK systems [10,11], real-time quantitative polymerase chain reaction (RT-PCR) [12–15], nucleic acid amplification tests (NAATs), immunofluorescence [16], enzymatic immunosorbent assays (ELISAs) [17,18] and side treatment point flow immunological assays (POCs) [19,20]. These molecular methods are considered the standard approaches for detecting the presence of viral components (genetic and/or protein material) in potentially infected individuals. However, in some cases, they may give rise to false negative results if the viral RNA charge at the time of detection is insufficient. For example, hemagglutination inhibition assays [21] exhibit low specificity under a certain agglutination level and when the samples contain non-specific hemagglutination factors [22]. Immunoassays may provide information on the status of ongoing viral infections and early exposure. Despite this, the main disadvantage of the aforementioned methods is the inability to identify the infection at a low viral charge, e.g., in the initial stage of the disease. This condition hardly depends on the immune response, which is detectable only several days after direct contact with the virus. In addition, most of the above-mentioned diagnosis processes have limitations, such as being time-consuming, labor-intensive and not reagent-free, as well as possessing poor sensitive and a slow detection process. These methods need sophisticated equipment and well-trained personnel to handle the tests. Therefore, complementary, reliable, fast, sensitive, easy-to-use and



**Citation:** Mancini, T.; Marcelli, A.; Lupi, S.; D'Arco, A. New Frontier in Terahertz Technologies for Virus Sensing. *Electronics* **2023**, *12*, 135. <https://doi.org/10.3390/electronics12010135>

Academic Editor: Costas Psychalinos

Received: 31 October 2022

Revised: 6 December 2022

Accepted: 12 December 2022

Published: 28 December 2022



**Copyright:** © 2022 by the authors. Licensee MDPI, Basel, Switzerland. This article is an open access article distributed under the terms and conditions of the Creative Commons Attribution (CC BY) license (<https://creativecommons.org/licenses/by/4.0/>).

cost-effective point-of-care diagnostics methods are highly desirable. In such circumstances, various bio-sensor platforms, based on electrical, mechanical [23], optical [24] and plasmonic [24–28] approaches, have shown promising and appealing applications ranging from laboratory to clinical/medical investigations, with a high potential in miniaturized, real-time and label-free sensing [28–31]. All biosensor-based approaches have a common schematic layout, as reported in Figure 1. A specific bioreceptor surface selectively adsorbs/captures the analyte of interest and then generates a signal (in the form of light, voltage, current, charge or mass change, variation of refractive index, etc.) as a result of the interaction between the bioreceptor and the analyte. The bio-recognition event results in constituting highly sensitive detection and discrimination signals. These data are converted by a transducer into another form of energy, and then amplified and processed in order to record a direct, measurable and readable signal, generally proportional to the amount of interaction between the analyte–bioreceptor. Biosensor-based approaches exploit different intrinsic chemical, electrical or energetic properties of bio-macromolecules constituting virus structure. For example, concerning the electrical-based approach, viral biological molecules capacitance or impedance have been studied and considered as significant discriminative quantities. For instance, as Al Ahmad and co-workers showed in their work, the electrical properties of viral suspensions depend upon protein, lipidic and envelope structures of the considered species; therefore, measurements of capacitance constitute a unique discrimination quantity. However, it has to be pointed out that only electrically polarizable virions can be detected and recognized with this method [32,33]. An innovative application of this electrical approach is reported in the study by MacCusprie et al. [34], who first exploited AC capacitance scanning probe microscopy to investigate biological samples, proving that different viruses have specific capacitance values. This is due to different capsid proteins and glycoproteins, which highly influence the dielectric properties defining the viral strain.

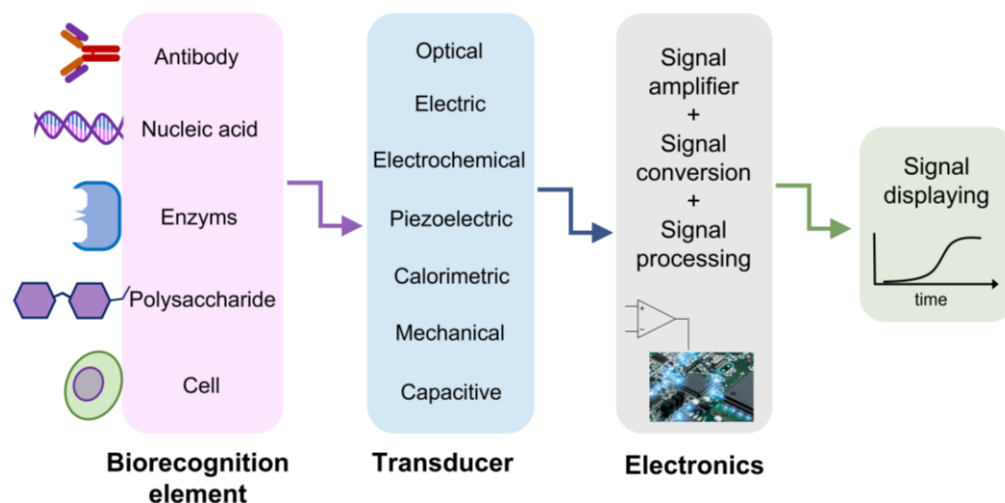


**Figure 1.** A schematic representation of biosensor structure. The biorecognition element is chosen to effectively catch the analyte of interest. The transducer reveals the presence of the analyte thanks to the variation of a physical quantity, depending on the approach exploited. The achieved signal is amplified, digitalized, processed and read on a display.

In this plethora of different techniques, another advantageous approach is represented by optical biosensors, which are essentially based on exploiting the different virus optical responses to an incident electromagnetic field. Different bio-macromolecular structures and compositions result in different refractive indexes and optical properties. Optical platforms have gained considerable attention for their potential in remote diagnosis schemes and their compatibility with physiological and serological solutions. Furthermore, within the optical-based sensor, a fundamental and essential role is played by the plasmonic approach,

which instead is based on specific materials resonances (e.g., the surface plasmons), whose properties, and, in particular, their characteristic frequencies, are modified when a virus is present on their surfaces.

In Figure 2, we report a graphical summary of the main detection approaches for virus sensing which are currently in use.

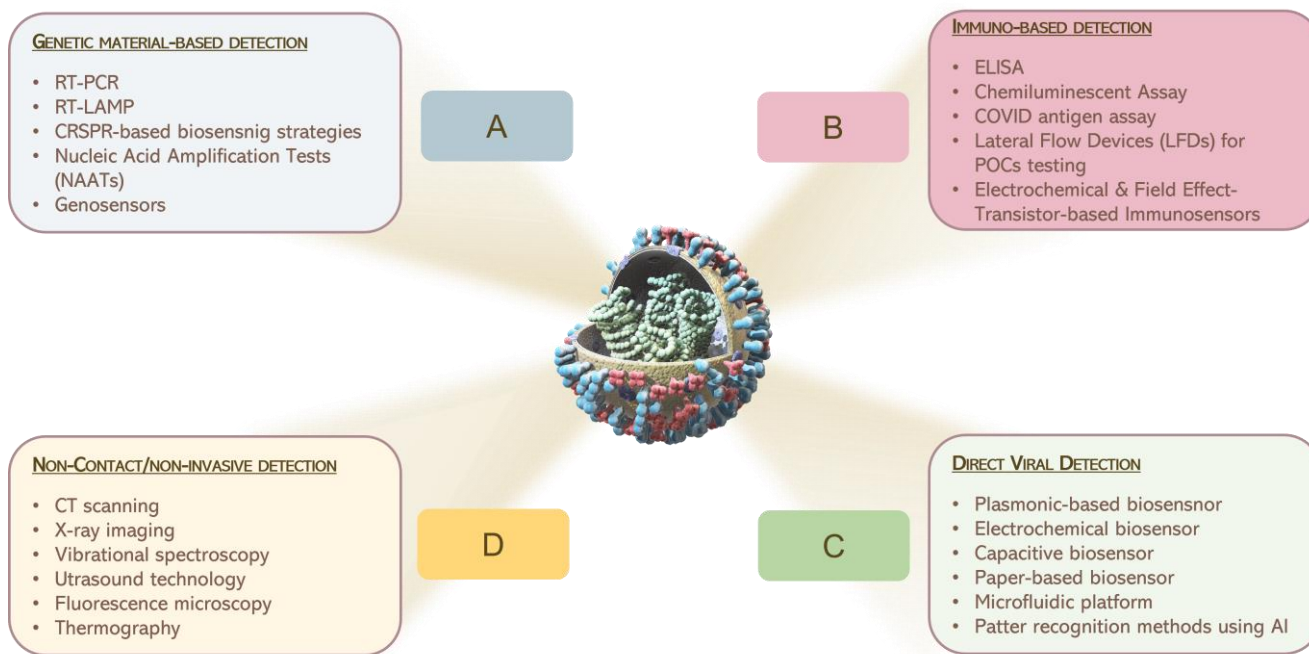


**Figure 2.** Graphical illustration of the main consolidated processes for the detection of pathogens, currently in use.

In this rich scenario, the emerging Terahertz (THz) technology is an ideal candidate for virus monitoring and detection purposes, offering various advantages which can be explored. The aim of this manuscript is to present the recent advances in THz biosensing for virus and viral particles. We summarize the pioneering studies that has paved the way for the application of THz radiation in this research field. Underlining the advantages and drawbacks of THz radiation and the related technologies, we highlight recent efforts and opportunities in virus sensing.

## 2. THz Technology for Virus Sensing

Despite the extensive attention given to microwave, infrared and visible regions, there is a small gap between microwave and infrared ( $0.1\text{--}10\text{ THz}$ ,  $3\text{--}330\text{ cm}^{-1}$ ), called the THz spectral range. This region of the electromagnetic spectrum has been often ignored because of the technological difficulties in THz generation and detection. In recent years, THz technology has grown, driven by improvements in sources, detector responses [35–42] and the availability of new materials with a strong THz response [43,44]. This has promoted the diffusion of THz research into various areas, e.g., air-quality and gas sensing [45–50], material sciences [42,44,51–54], microelectronics and security [55,56], agri-food quality [57], cultural heritage [58], in addition to biomedicine and bio-imaging [59–63]. For biomedical and biochemical issues, THz radiation is really appealing because of its low photon energy (around few meV,  $4\text{ meV @ }1\text{ THz}$ ), and too low to heat materials and/or induce atom/molecule ionization; therefore, it enables non-destructive and non-ionizing sensing [64]. This is in contrast with other spectroscopic techniques, including ultraviolet or X-rays, where high-energy photons ( $\gg\text{eV}$ ) induce damage to the bio-sample [64]. In addition, THz radiation, characterized by low photon energy, is associated with energy

levels matching low-frequency vibrational modes, including the collective vibrations of intermolecular and intramolecular interactions, such as hydrogen bonds [65], the phonon modes of crystalline molecular solids and vibrations of many macromolecules. In these circumstances, THz spectroscopy has been employed to investigate low-frequency vibrational modes of amino acids and proteins, due to its sensitivity to intermolecular interactions, such as hydrogen bonds, which in turn are dependent on molecular conformations and surrounding environments [66,67]. Therefore, THz radiation directly identifies a material's spectral properties constituting its molecular fingerprint, offering, in this way, a chemical specificity to imaging and spectroscopy experiments, in a label-free, non-contact and non-invasive mode [59,68,69]. Moreover, it is worth to point out that non-polar materials (such as paper, cloths and plastic) are usually transparent in the THz range [55,70,71]. In contrast, the high sensitivity to polar molecules, such as water (absorption coefficient around  $220\text{ cm}^{-1}$  for pure water @ 1 THz), and the low spatial resolution are the main drawbacks of THz radiation [72,73]. In fact, the extreme absorption, shown by THz radiation for polar molecules, specifically water, restricts the penetrability of THz waves from tens to hundreds of microns in hydrated samples. The diagnostic capability, especially in the case of biomedical applications in vivo or on fresh tissues, is then reduced. Nevertheless, the high sensitivity of water content can be used like an endogenous marker for the differentiation between fresh healthy and pathological tissues and preventing a wider range of applications in biology [69,74]. Referring to THz spectroscopy, many layouts and materials are used for THz signal collection [75–77], showing high performance in terms of the signal-to-noise ratio (SNR) and coherent detection mode. Because THz spectroscopy is insensitive to the thermal background, it has a high SNR, not requiring the use of cooled detectors [78]. Concerning the coherent detection mode, the temporal profile of THz electric field is directly recorded. Therefore, both amplitude and phase of the THz pulse electric field can be simultaneously measured, and the optical parameters, including the sample absorption coefficient and refractive index, can be estimated without using Kramers–Kronig relations [79]. In Table 1, major THz technology features are reported; the advantages and disadvantages are summarized and listed to have an overall view on its potential in terms of detection and discrimination.

**Table 1.** Summary of THz spectroscopy. Advantages and disadvantages as a detection tool.

Advantages	Disadvantages
Low-energy photon	Low spatial resolution (hundreds $\mu\text{m}$ )
No-inflammable	Strong water absorption ( $220\text{ cm}^{-1}$ @ 1 THz)
No-ionizing radiation	Limited penetration inf fresh tissue
Sensitive to polar molecules	
Coherent detection	
No sample pre-treatment	

In spite of the constraints listed above, several findings have been carried out on biological materials [69,79,80]. Concerning the low spatial resolution, THz radiation suffers from poor spatial resolution due to its large wavelength ( $\lambda = 300\ \mu\text{m}$  @ 1 THz) [69,81]. The lateral dimensions of the typical viral pathogens range between 20–300 nm, thus their detection is very challenging because of their sub-wavelength dimensions [82]. The main obstacles for pathogenic monitoring are underlined by the work of Lee and co-workers [83].

They exploited THz spectroscopy to evaluate the optical parameters of H9N2 virus samples in the frequency range 0.2–2.0 THz. The authors did not show any identifiable spectral features between the absorbance of the freeze-dried virus pellet or the substrate (Figure 3). The weak sensitivity, low detectability and poor chemical selectivity due to the super-position of many biological vibration modes, essentially related to the protein content, prevented the use of THz for virus sensing. However, when a direct assessment fails, indirect virus detection is still possible. Indeed, the probing for antibody–antigen binding properties through THz spectroscopy is more sensitive compared to the standard

ELISA [84,85]. One example is the extensive work by Sun et al. [86] on the H9 HA glycoprotein of avian influenza and its binding properties for specific (F10) and non-specific antibodies.

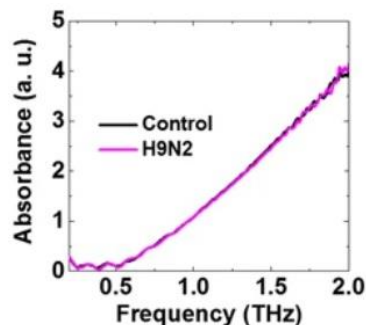


**Figure 3.** A comparison of the absorption spectra of a pellet of H9N2 virus (violet line) and a control sample (black) without the virus [83]. Reprinted from [83].

Although direct detection is preferable, indirect methods may be favorably to overcome THz limitations and make THz technologies available for pathogenic sensing and biomolecular applications, e.g., in efficient graphene-based sensors, in micro-fluidic chips or in novel meta- and nano-materials [83]. Zhou et al. reported fascinating optoelectrical properties for graphene and predicted the possibility to raise the limit of detection (LOD) of biomolecules using graphene plasmons [82,85]. On the other hand, one of the challenges for biosensing is to perform measurements on minimal amounts. In this context, micro-fluidic chips are suitable for investigation in different physiological and serological environments [87]. They are able to select extremely small amounts of liquid and trap the molecules in the micro-fluidic channel, thus limiting the strong THz water absorption and providing very concentrated measurements. Devices based on meta- and nano-materials [85,88–94] have gained popularity as promising protein and DNA detection platforms [24,95–98] because of their operational simplicity, compactness and their attractive electromagnetic properties, such as the excitation of surface plasmon polaritons (SPPs) [99–102] and the localization and enhancement of the electric field associated with the incoming radiation. Firstly, O’Hara et al. [103] demonstrated that a THz metamaterial, structured with a double split ring on a Si substrate, provides a high sensing capability and a significant enhancement of the sensitivity for THz metamaterials fabricated on thin and low-permittivity substrates [104,105]. Meta- and nano-platforms are artificially structured devices, made up of several unit cells or individual elements with sub-wavelength sizes. Some examples of these selected geometries for metamaterial unit cells are reported in Figure 4. In the THz field, these materials may have single- or multi-resonance frequencies  $f_0^n$ , strictly depending on the geometrical properties [106–108], orientation and arrangement of the unit cells. Sample deposition on meta- and nano-structured devices induce a variation in their dielectric properties [106–108], including the shifting of their resonance frequencies. Being proportionally sensitive to the frequency shift, an appropriate design of the unit cell area is crucial to enhance the detection capability [109–111].

Thus, the local dielectric changes generated by biological samples, such as viruses, may be successfully detected. In addition, since very thin water layers are required (a few tenths of a  $\mu\text{m}$ ), these layouts easily overcome the limitation imposed by the strong THz water absorption [109]. The sensor specificity or biological selectivity may be increased with functionalization, e.g., anchoring the bio-analytes and/or bio-components of interest onto the meta- or nano-material platforms. Various approaches have been proposed: functionalization with alkanethiol molecules of well-ordered covalently bonded monolayers, the generation of hydroxyl groups by oxygen plasma or the surface chemical modifications using silane and silanol chemistries, the  $\text{CO}_x\text{-H}$  modification, the anchoring and/or the decoration with antigens [110–113].

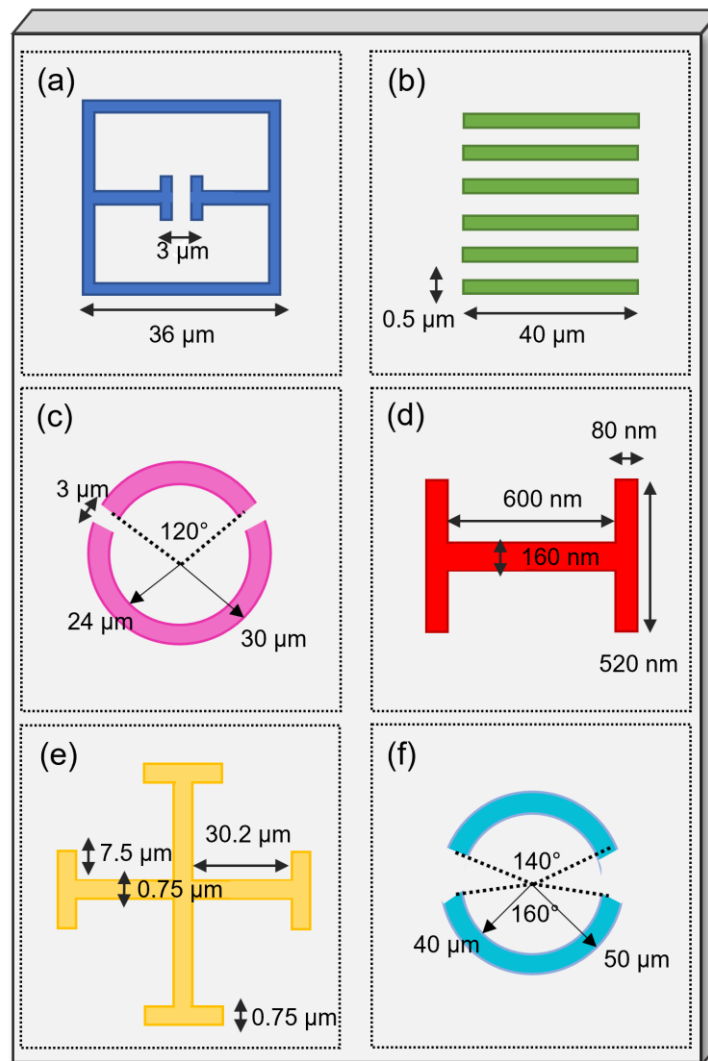


**Figure 4.** Examples of different geometries adopted for metamaterial unit cells. (a) split-ring resonator [82], (b) rectangular slot [83], (c) double-split ring [114], (d) H-shaped resonator [115], (e) planar Jerusalem cross [100] and (f) asymmetric split-ring resonator. (original figure).

### 3. Recent Advances in THz-Based Sensing and Detection for Viral Pathogens

One of the earliest pioneering studies focused on THz virus sensing was carried out by Park et al. [82]. They combined THz-TDS with a fabricated THz split-ring resonator, shown in Figure 5a. Metamaterial platforms for virus sensing at low densities were prepared by e-beam lithography on a 1 mm thick quartz substrate. Subsequently, Cr (3 nm) and Au (97 nm) metal films were deposited by e-beam evaporation, defining the electrical split-ring resonators with a line width of 4 μm, outer dimensions of 36 μm × 36 μm and various gap sizes with an array periodicity of 50 μm.

Tests were performed to detect two types of viruses, with sizes ranging from 60 nm (PRD1) to 30 nm (MS2), deposited at low densities on the metamaterial surface. The presence of the viral pathogen within the capacitor gap changed the resonance frequency and optical parameters. For a 40 μm thick layer, the dielectric constants for both viruses were assessed. Successively, the authors demonstrated the relation between the resonance frequency shifts and the virus surface density, observing an increasing frequency shift in surface density until saturation. Actually, the sensitivity increased by about 13 times as the gap width in the metamaterial decreased from 3 μm to 200 nm. Promising results were achieved by the proposed by Cheng and coworkers for protein detection with a metasurface

with an asymmetric split-ring resonator pattern and sensitivities around 160 GHz/RIU and 240 GHz/RIU [116]. Although, this approach is aimed to detect proteins, an extension based on the interaction of receptors with membrane proteins is feasible for applications detecting viral pathogens.

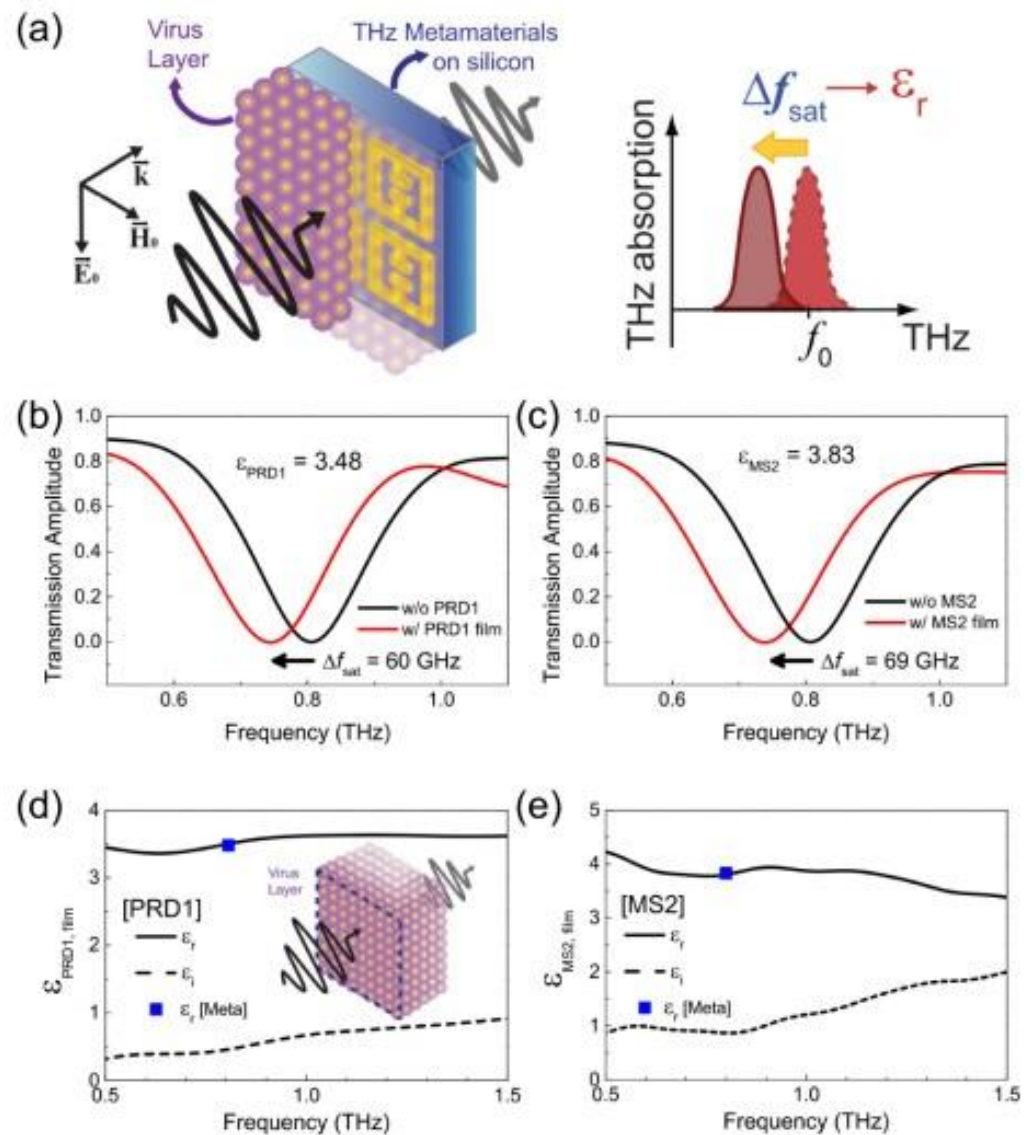


**Figure 5.** (a) The layout of dielectric constant measurements using a THz metamaterial sensor. THz transmission vs. frequency, with and without the deposition of the layer of (b) PRD1 and (c) MS2 viruses. The dielectric constants of 3.48 and 3.83 are estimated from the resonant frequency shift, for PRD1 and MS2, respectively. Frequency-dependent complex dielectric constants vs. frequency are reported for (d) PRD1 and (e) MS2 layers. The thicknesses of the PRD1 and MS2 layers were 300  $\mu\text{m}$  and 150  $\mu\text{m}$ , respectively. Reprinted with permission from [82] © The Optical Society.

Hong et al. [109] fabricated hybrid slot antennas on a quartz substrate garnishing them with silver nanowires (20 nm in diameter and 1–5  $\mu\text{m}$  in length) and tested them on PRD1 virus droplets. They observed that the presence of nanowires enhanced the sensitivity. In particular, the hybrid chip exhibited a 2.5-fold increase in sensitivity compared to the bare chip (33 GHz· $\mu\text{m}^2$ /particle instead of about 13 GHz· $\mu\text{m}^2$ /particle). Various groups performed finite-difference simulation of the optical parameters in the time domain using different metamaterials and unit cell geometries. In particular, Lee's team explored the

possibility of THz virus sensing for AI virus subtypes, such as H1N1, H5N2 and H9N2. They tested a device comprising rectangular nano-antennas (see Figure 4b) on a silicon wafer patterned with gold (150 nm) fabricated by e-beam lithography. Each virus sample produced different changes in dielectric properties and resonance frequency shifts with respect to the substrate, suggesting a method for discrimination. In addition, observing the H9N2 THz transmittance by varying the virus concentration, the authors found a linear decrease in intensity at the resonance frequency as the concentration increased, as reported in Figure 6a.

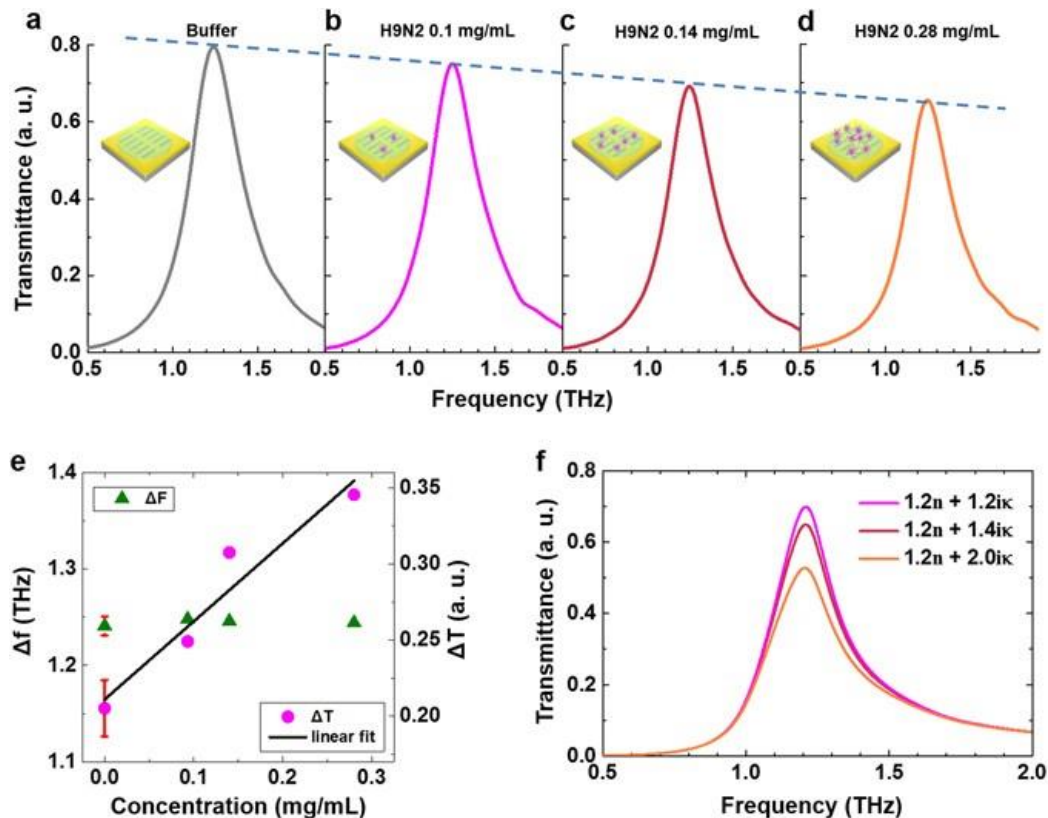


**Figure 6.** H9N2 transmittance vs. frequency by varying the viral pathogen concentration. (a) Buffer ( $0 \text{ mg mL}^{-1}$ ), (b)  $0.10 \text{ mg mL}^{-1}$ , (c)  $0.14 \text{ mg mL}^{-1}$ , and (d)  $0.28 \text{ mg mL}^{-1}$ . (e) Variation in the maximum values of the normalized transmittances ( $\Delta T$ , magenta closed circle) and shifted resonance frequency ( $\Delta f$ , green closed triangle) for the H9N2 virus in different concentrations. The red bar indicates the errors bar due to the buffer solution and the black line is the linear fitting of the transmittance change vs. concentration. (f) Results of the numerical simulations using the finite-difference time-domain (FDTD) method of transmittances for three different model samples with various compositions of dielectric constants ( $n$  and  $\kappa$ ). Reprinted from [83].

Lee and co-workers found good agreement among the experimental results and the simulated behavior of the sensing platform varying the complex refractive indexes (see Figure 6f). The same results were confirmed by Cheng and co-authors [100,101], that used a planar Jerusalem cross structure (see Figure 4e). They modeled a sensor with  $5 \mu\text{m}$  thick samples by varying the optical properties associated with the viruses, looking at the resonance frequency shifts and absorption changes.

The extraordinary properties of graphene in the THz regime inspired various sensor designs. Taking advantage of the ease of tunability of its operating frequencies by varying the electromagnetic field and/or chemical doping, some narrow and multi-band absorbers can be designed to operate with high sensitivity in the THz spectral window. A smart and compact graphene-based absorber with a dual absorption peak for biosensing applications

was recently proposed by Karthikeyan et al. [92]. The absorber, schematically reported in Figure 7, works in dual operating bands at 5.1 THz and 11.7 THz. It may change the resonance wavelength to drive the absorption frequencies tuning the graphene chemical potential. Due to the confinement of the graphene surface plasmon it exhibits an extremely precise and condensed absorption peak.

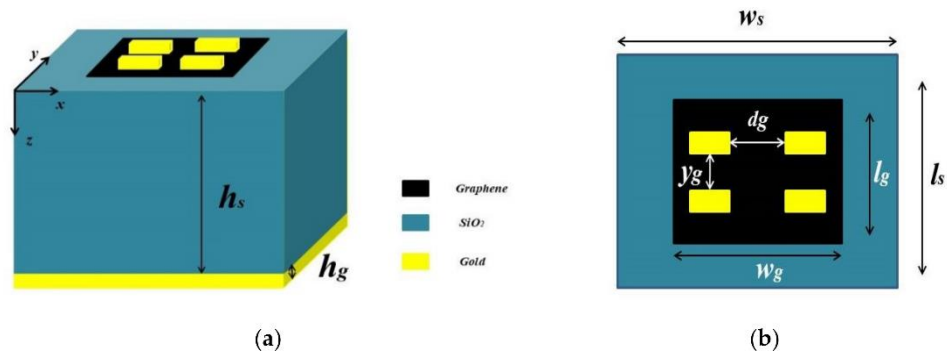


**Figure 7.** Absorber unit cell structure is depicted with a single sheet of graphene and four small sized gold bars. (a) 3D view: the absorber consists of a gold meta-array at the top. Gold bars with height  $h_g$  and width  $w$  are placed in the form of a  $2 \times 2$  array. Beneath the gold bars and above the substrate is a graphene layer growing on a silicon dioxide ( $SiO_2$ ) substrate with thickness  $h_s$  and  $\epsilon_r = 2.25$ . To reduce the transmission, an additional gold layer with thickness  $h_g$  is used. (b) 2D top view. Reprinted from [92].

Using the sensing medium with various refractive indexes, the authors first simulated the absorber working for glucose detection achieving a maximum sensitivity of 2.08 THz/RIU and 4.72 THz/RIU in sensing water with 25% glucose at the resonant peaks I and II, respectively. Extending the simulation to malaria identification (with refractive indexes 1.383 and 1.373 in trophozoite and schizont phases) and setting to  $2 \mu m$  analyte thickness to enhance the sensing capability, performances of the graphene-based sensor reached the sensitivity values of 1.76 THz/RIU and 3.72 THz/RIU at the resonant peaks I and II, respectively. Its good responsiveness and the standard fabrication make it a suitable candidate for biomedical applications.

A different approach was proposed by Amin and colleagues [117,118]. They employed a graphene-based plasmonic metasurface and exploited the reflected light polarization as the detection signal and the tunability of the resonance frequency. The unit cell had a split-ring structure, where the perpendicular graphene slices had slightly different sizes, and the substrate was made from quartz, designed to generate chiral or helicoidal plasmon (reported in Figure 8). Chiral and helicoidal plasmons result in producing elliptically polarized electric fields in the THz domain. Reflection coefficient matrix elements  $|R_{xx}|$  and  $|R_{yx}|$  of the metasurface changed as the analytes refractive index changes, determining an elliptical polarization of reflected light whose ellipticity depends on the virus species. The system response was proven with three different influenza viral strains, H1N1, H5N2 and H9N2. They numerically simulated its response considering a viral sample layer of  $5 \mu m$  and the viral optical properties reported in the literature. Viral sample concentrations and refractive indexes are listed in Table 2.

**Table 2.** Synthetic summary of THz technology characteristics. Advantages and disadvantages as a detection tool.

Strain Name	Protein Concentration	Complex Refractive Index
H1N1	0.54 (mg/mL)	$n + 1.4 ik$
H5N2	0.2 (mg/mL)	$n + ik$
H9N2	0.28 (mg/mL)	$1.2 n + 1.4 ik$

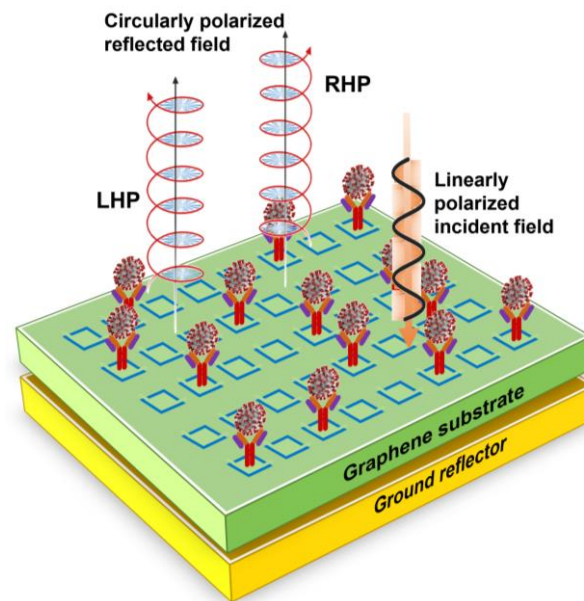


**Figure 8.** Metasurface sensor based on chiral-localized surface current. A monochromatic linearly polarized light impinges on the patterned surface. This is properly functionalized with antibody or bioreceptor protein able to catch the virus of interest. Depending on the refractive index of the considered analyte–antibody system, the ellipticity of the circularly polarized reflected field changes, providing the detection signal.

Two resonant detection frequencies were considered, 1.364 and 1.717 THz. H9N2 reflected light polarization differs the most from the other viral strains, H1N1 and H5N2, which instead showed similar spectral responses, having a similar refractive index, apart for a small difference in the imaginary part value (extinction coefficient). Despite this, their polarization states at both resonance frequencies were clearly distinguishable, suggesting this technique could efficiently discriminate similar viral strains.

Moreover, the use of gold nanoparticles (AuNPs) has been introduced into the THz spectral range in combination with metamaterial biosensors [82,119]. In fact, as a consequence of the integration of a THz plasmonic metasurface and AuNPs, the sensor LODs can be increased achieving large resonance figures. Ahmadivand et al. designed a toroidal metamaterial [119–122] biosensor to detect the envelope protein of the ZIKA virus, by measuring the spectral shift of the toroidal resonance [119,120]. They exploited the effect induced by the addition of AuNPs, observing at low concentrations an increase of 100-fold in the sensor response. The same authors used hybrid 2D microstructures of Fe and Ti to design a set of asymmetric split resonators supporting ultra-strong and narrow magnetic toroidal moments in the THz spectral region. They achieved a LOD around 24.2 pg/mL with a sensitivity of 6.47 GHz/log(pg/mL).

In addition, to overcome the typical drawbacks of conventional metasensors, they investigated the possibility of low molecular weight biomolecule detection at low densities [121,122]. They adopted a miniaturized plasmonic immunosensor, based on the concept of toroidal electrodynamics confining plasmonic modes with ultra-narrow line shapes in the THz spectral region. Instead, toroidal dipole-resonant metasurfaces exhibited unconventional spectral properties, such as high sensitivity to the refractive index variations, low-radiative losses, and low mode volumes through the robust confinement of electromagnetic fields. Ahmadivand’s group proved and verified the proof-of-concept THz toroidal metasensors for the detection of heavy hormones, drugs, organisms, enzymes, envelope proteins of specific viruses (Zika virus envelope protein with a molecular weight of ~13 kDa) and antibiotic molecules (Kantrex,  $C_{18}H_{36}N_4O_{11} \times H_2SO_4$ , with the molecular weight of ~600 Da) at very low concentrations [119,120,123]. To improve the binding properties of the targeted biomolecules to the device’s metasurface, they developed functionalized

colloidal AuNPs conjugated with associated bioreceptors to bind respective analytes [124]. Specifically, they combined the toroidal dipole mode, using a quasi-infinite metasurface and a protocol based on functionalized AuNPs conjugated with monoclonal antibodies specific to the SARS-CoV-2 spike glycoprotein subunit 1 (S1). They measured resonance shifts for different protein concentrations. In particular, this sensor was able to detect the presence of SARS-CoV-2 viral proteins with a significantly low LOD, around  $\sim 4.2$  fM.

Moreover, Shi et al. [125] considered an all dielectric metasurface with a split half-cylinder array configuration with dual resonant bands. They combined this with AuNPs conjugated with a specific antibody, Anti-HA, in solution and dispersed onto the surface. This procedure formed an immunobinding with the HA antigen of human influenza. Results for polarized incident THz radiation showed that, in particular the highest resonance frequency undergoes an overall shift of 87.5 GHz as the concentration of HA antigen increased (from 20 to 50  $\mu\text{g}/\text{mL}$ ). This value was around two times the frequency shift resonance peak if AuNPs were not employed in the functionalization, measured to be 43.75 GHz. Therefore, the sensitivity of the system was calculated for both resonance frequencies, both polarizations and with or without AuNPs. All in all, the highest value of sensitivity was obtained for the  $y$ -polarization and the highest resonance frequency ( $S = 2.96$  GHz mL/nmol) when AuNPs were used. In addition, the use of gold magnetic nanoparticles (GMNPs) has been explored. They not only possess the advantage of superparamagnetic particles to enable the isolation and/or extraction of target nucleic acids [114], but also the outstanding property to enhance the capture of targets in the surrounding medium of the THz metamaterials and improve the sensor LODs. A recent application was proposed by Li et al. [114]. They fabricated a flexible THz metamaterial-based biosensor for the highly sensitive and selective detection of hepatitis B virus (HBV) DNA in clinical serum samples, using a gold magnetic nanoparticle-mediated rolling circle amplification (GMNPs@RCA) sandwich assay under isothermal conditions. This THz biosensing strategy is reported in Figure 9.

Exploiting the high amplification efficiency induced by the RCA under isothermal conditions, as well as the intrinsic high sensitivity of the gold-mediated nanoparticles in association with the THz metasurfaces, HBV DNA serum as low as  $1.27 \times 10^2$  IU/mL was detected by THz spectroscopy [114].

High sensitivity and quantitative detection were proposed by Niu et al. [126] for the SARS-CoV-2 S1 subunit. Their approach was different compared to the work of Ahmadi-vand and co-workers [124], where a combination of toroidal dipole mode and AuNPs conjugated to functionalized monoclonal antibodies was used to drive the LOD to the fM domain. For high-accuracy detection of the SARS-CoV-2 S1 they integrated THz-TDS, THz metamaterials and biological functionalization within a THz metamaterial biosensor made with a three-split-ring (TSR) resonator, as shown in the layout of Figure 10. In their experiments authors reached a LOD of less than 5 ng and observed that the resonance frequency shifts and the variation of FWHM were proportional to the S1 concentration in the solution. In detail, Figure 11A shows the measured transmittances of the S1 protein samples at different concentrations in the spectral region between 0.55–0.85 THz. The frequency shifts are observed vs. concentration. They fit linearly with concentrations ranging from 1 to 30  $\mu\text{g}/\text{mL}$ , and can be described by  $\Delta f = 5.563 + 1.084 \cdot x$ , as displayed in Figure 11B. The increase in the concentration results in the increase in the filling fraction  $k$  and the effective dielectric constant  $\epsilon_{\text{eff}}$ . Meanwhile, with increasing S1 protein concentration, the FWHM significantly increased due to the absorption of the analyte (see Figure 11C).

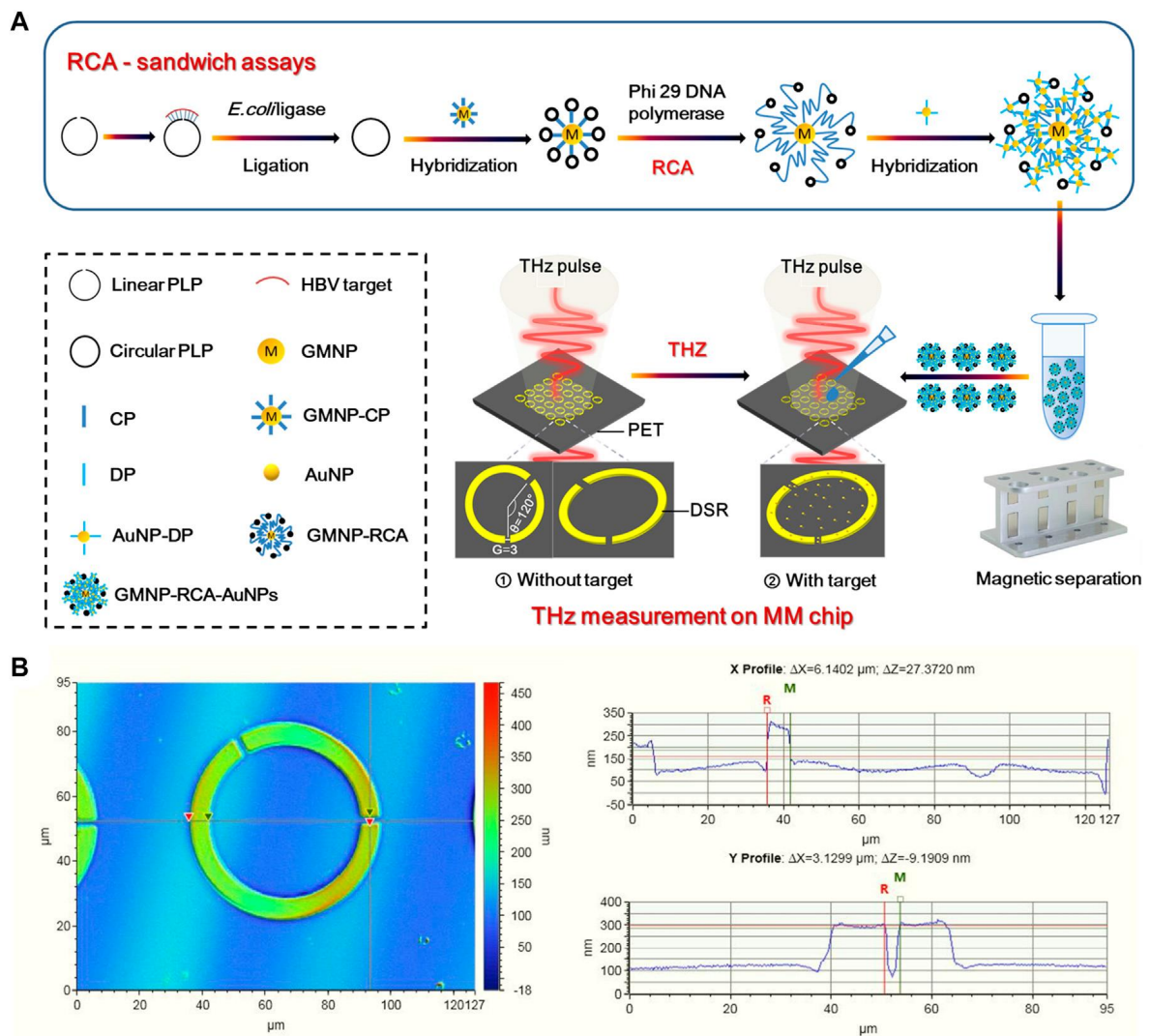


**Figure 9.** A visual summary of the THz biosensing strategy, adopted by Li et al. for HBV DNA sensing. (A) Graphical description of the THz biosensor chip for HBV DNA detection based on the GMNPs-RCA-AuNPs sandwich assay. To increase the LOD, the metamaterial metal split-ring (SR) resonators are composed of double asymmetric splits fabricated on an ultra-thin PET substrate with low intrinsic loss. The DSR sensor features strong sensing characteristics due to the resonance shift loaded with the dielectric material. (B) Characterization of the DSR cell. Reprinted from [114].

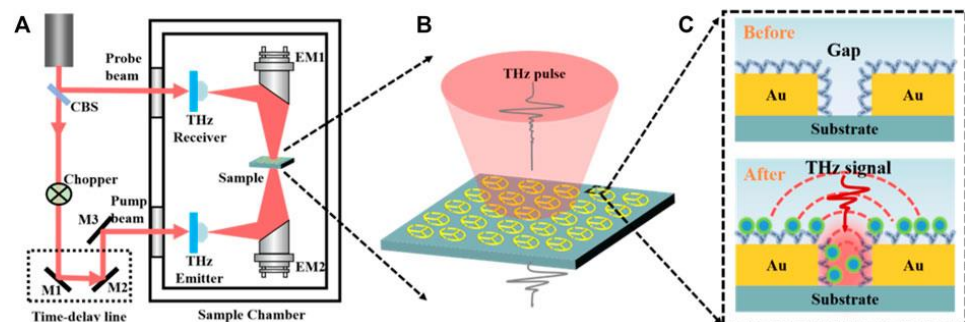


**Figure 10.** Graphical illustration of the experimental setup and the sample adopted by Niu and co-authors: (A) THz-TDS setup, (B) magnified picture of the sensor, and (C) schematic representation of Au structures and air gaps before and after the combination of the S1 protein. Reprinted from [126].

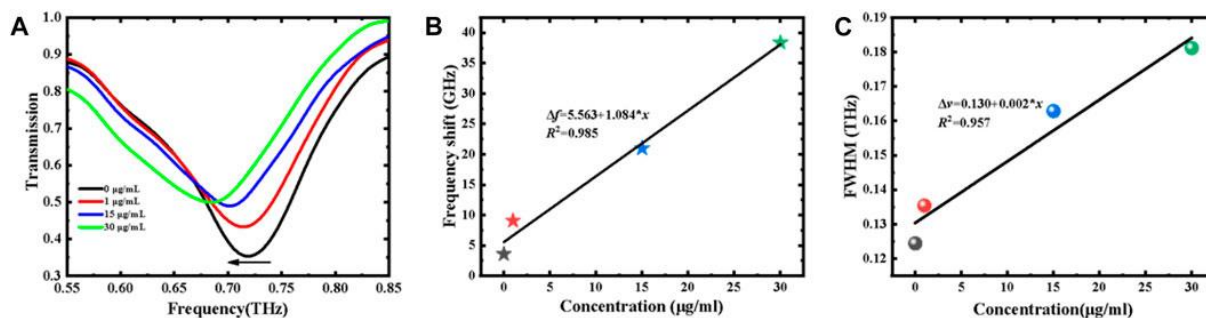


**Figure 11.** (A) Measured transmittances of the S1 protein at different concentrations. (B) Resonance frequency shifts and (C) FWHM variation vs. concentration. Reprinted from [126].

Numerical simulations were performed varying the sensor and analyte parameters (thickness, quantity, position and refractive index of the analyte aggregates) with the aim to confirm the sensing characteristics experimentally observed and provide further insight into the sensing mechanisms. Recently, triggered by great efforts in computer sciences, various groups have performed computer simulations of the sensor behavior to predict and/or explain the experimental results. As mentioned in the text, the accessibility to calculation and simulation systems has allowed exploration of the performance of sensors vs. the geometric parameters, reducing and limiting the time and effort required in the preparation and costs. High responsiveness and LODs can now be predicted. Recent works, in fact, have explored and addressed new sensor designs starting from numerical simulations [92,127]. Several groups [83,100,115] adopted finite-difference time-domain simulation modelling the virus samples. In particular, three samples of avian influenza virus (H1N1, H5N2 and H9N2) were modeled as  $\sim \mu\text{m}$  thick layers, composed by homogeneous dielectric clads. For each of them, the complex refractive index  $N$  was estimated, in addition to the two coefficients,  $\alpha$  and  $\beta$ , relative to the real and imaginary parts, respectively, characteristic of viral properties, such as different virus types and concentrations [83,100].

#### 4. Future Trends and Conclusions

The substantial need for deployable technologies for quick and effective viral detection on a large scale has grown and it is continuously increasing, not only because of the recent pandemic events. Although various molecular (RT-PCR, bDNA, RTLAMP, etc.) and immuno-based techniques are currently available and successfully used, they still remain complex and difficult to apply on a large scale and are not rapid enough to ensure high-precision diagnostic tests at low concentrations.

In this framework, since these methods are equitably limited, there is a need for new, accurate and highly sensitive alternative solutions. In such circumstances, various biosensor platforms have been proposed, based on electrical, mechanical [24], optical [23] and plasmonic [23–27] approaches. All are promising applications suitable for laboratory and clinical/medical investigations, with a high potential for compact, portable, real-time and label-free sensing [26–30]. Among these different genres of approaches, biosensor platforms based on optical detection have gained considerable attention, such as THz spectroscopy, also in combination with THz nano- and metamaterials. The recent progress in THz technology and the advantages offered by this non-ionizing radiation, discussed in this review, make this electromagnetic domain ideal for biosensing applications, such as virus detection, complementing or enhancing existing solutions. This contribution outlines existing THz-based virus sensing platforms and emphasizes the possibility to detect and identify viruses with THz waves. We briefly focused on the advantages of THz technology and sensing, such as THz-TDS, outlining also its drawbacks, such as limited sensitivity to monitor and/or identify viral pathogens. Although THz spectroscopy has been used for the study of the optical properties, such as refractive index and absorption coefficient, of different genres of pathogens, the THz wavelength are much larger than the viruses

and viral particle sizes. This results in very low spatial resolution and reduced sensitivity. However, the incredible advancements in optics, make it possible to maximize the interaction between radiation–biomaterial utilizing plasmonic and metamaterial-based biosensors. Here, we thoroughly dealt with the existing THz techniques adopted for THz virus sensing, including the advantages provided by meta- and nano-THz sensors. Meta- and nanomaterials, operating in the THz frequency region, are an appealing alternative and guarantee a great potential for high-speed, on-site and label-free point-of-care virus detection. Some previously reviewed plasmonic platforms, such as planar metal-dielectric biosensors, need simple and smart fabrication techniques to reach low LODs. We explored pioneering studies in THz virus sensing and reported the technological efforts in THz metamaterial optical biosensors, highlighting the flexibility of a variety of geometric structures, their sensitivity and LODs for various viruses. However, the strong potential of THz-based virus detection is still in its initial development steps and far from clinical use. Nevertheless, recent technological improvements in manufacturing and miniaturizing THz layouts promise to enhance the performances of meta- and nano-sensors, achieving sensitivities higher than traditional/conventional devices and even to permit remote location and control. Finally, recent machine learning applications have garnered great acclaim in several scientific fields, including sensor design, where the behavior of integrated metamaterial systems has been explored [127]. Deep learning methods have also been successfully used to predict potential correlations among plasmonic geometric structures, their optical parameters and the resulting resonance spectra [128]. Research based on new photonic materials, such as topological insulators and quantum photonics devices, offer promising ideas for THz biosensing.

In this framework of continuous evolution, we believe that THz-sensing technologies, although still in their infancy, will continue to grow achieving a relevant position in the biosensing area in the future.

**Author Contributions:** Conceptualization, A.D. and S.L.; writing—original draft preparation, A.D. and T.M.; writing—review and editing, A.D., T.M., A.M. and S.L.; supervision, S.L. and A.M.; project administration, S.L. and A.M.; funding acquisition, S.L., A.M. and A.D. All authors have read and agreed to the published version of the manuscript.

**Funding:** This review was supported by the Ph. D. funding in the framework of Programma Operativo Nazionale (PON)—Ricerca e Innovazione 2014–2020—Azione IV.5-Dottorati su tematiche green. Moreover, this work was supported by the funding BRIC-INAIL project ID 07/2019; NATO Science for Peace and Security Programme under grant No. G5889—“SARS-CoV-2 Multi-Messenger Monitoring for Occupational Health & Safety-SARS 3M”, LazioInnova “Gruppi di Ricerca 2020” of the POR FESR 2014/2020-A0375-2020-36651 project entitled “DEUPAS—DEterminazione Ultrasensibile di agenti PATogeni mediante Spettroscopia”, and finally by the “Avvio alla Ricerca Sapienza 2022” Grants, entitled “Tracking di SARS-CoV-2 aerodisperso nei luoghi di lavoro mediante spettroscopia vibrazionale ultrasensibile” and “Rivelazione ultra sensibile di composti organici volatili in atmosfera attraverso spettroscopia vibrazionale”.

**Data Availability Statement:** Not applicable.

**Conflicts of Interest:** The authors declare no conflict of interest.

## References

1. Campi, G.; Perali, A.; Marcelli, A.; Bianconi, A. Sars-CoV-2 world pandemic recurrent waves controlled by variants evolution and vaccination campaign. *Sci. Rep.* **2022**, *12*, 18108. [[CrossRef](#)] [[PubMed](#)]
2. Tsongalis, G. Branched DNA technology in molecular diagnostics. *Am. J. Clin. Pathol.* **2006**, *126*, 448–453. [[CrossRef](#)] [[PubMed](#)]
3. Udugama, B.; Kadhiresan, P.; Kozłowski, H.N.; Malekjahani, A.; Osborne, M.; Li, V.Y.C.; Chen, H.; Mubareka, S.; Gubbay, J.B.; Chan, W.C.W. Diagnosing COVID-19: The disease and tools for detection. *ACS Nano* **2020**, *14*, 3822–3835. [[CrossRef](#)] [[PubMed](#)]
4. Long, Q.-X.; Liu, B.-Z.; Deng, H.-J.; Wu, G.-C.; Deng, K.; Chen, Y.-K.; Liao, P.; Qiu, J.-F.; Lin, Y.; Cai, X.-F.; et al. Antibody responses to SARS-CoV-2 in patients with COVID-19. *Nat. Med.* **2020**, *26*, 845–848. [[CrossRef](#)]
5. Yan, C.; Cui, J.; Huang, L.; Du, B.; Chen, L.; Xue, G.; Li, S.; Zhang, W.; Zhao, L.; Sun, Y.; et al. Rapid and visual detection of 2019 novel coronavirus (SARS-CoV-2) by a reverse transcription loop-mediated isothermal amplification assay. *Clin. Microbiol. Infect.* **2020**, *26*, 773–779. [[CrossRef](#)]

6. Carter, L.; Garner, L.; Smoot, J.; Li, Y.; Zhou, Q.; Saveson, C.J.; Sasso, J.M.; Gregg, A.C.; Soares, D.J.; Beskid, T.R.; et al. Assay techniques and test development for COVID-19 diagnosis. *ACS Cent. Sci.* **2020**, *6*, 591–605. [[CrossRef](#)]
7. Sabalza, M.; Yasmin, R.; Barber, C.; Castro, T.; Malamud, D.; Kim, B.; Zhu, H.; Montagna, R.; Abrams, W. Detection of zika virus using reverse-transcription lamp coupled with reverse dot blot analysis in saliva. *PLoS ONE* **2018**, *13*, 019239. [[CrossRef](#)]
8. Bastos, M.L.; Tavaziva, G.; Abidi, S.K.; Campbell, J.R.; Haraoui, L.P.; Johnston, J.C.; Lan, Z.; Law, S.; MacLean, E.; Trajman, A.; et al. Diagnostic accuracy of serological tests for covid-19: Systematic review and meta-analysis. *BMJ* **2020**, *370*, m2516. [[CrossRef](#)]
9. Broughton, J.; Deng, X.; Yu, G.; Fasching, C.; Servellita, V.; Singh, J.; Miao, X.; Streithorst, J.; Granados, A.; Sotomayor-Gonzalez, A.; et al. CRISPR-cas12-based detection of SARS-CoV-2. *Nat. Biotechnol.* **2020**, *38*, 870–874. [[CrossRef](#)]
10. Kellner, M.; Koob, J.; Gootenberg, J.; Abudayyeh, O.; Zhang, F. Sherlock: Nucleic acid detection with CRISP nucleases. *Nat. Prot.* **2019**, *14*, 2986–3012. [[CrossRef](#)]
11. Patchsung, M.; Jantarug, K.; Pattama, A.; Aphicho, K.; Suraritdechachai, S.; Meesawat, P.; Sappakhaw, K.; Leelahakorn, N.; Ruenkam, T.; Wongsatit, T.; et al. Clinical validation of a Cas13-based assay for the detection of SARS-CoV-2 RNA. *Nat. Biomed. Engin* **2020**, *4*, 1140–1149. [[CrossRef](#)] [[PubMed](#)]
12. Pan, Y.; Zhang, D.; Yang, P.; Poon, L.L.M.; Wang, Q. Viral load of SARS-CoV-2 in clinical samples. *Lancet Infect. Dis.* **2020**, *20*, 411–412. [[CrossRef](#)] [[PubMed](#)]
13. Jartti, T.; Soderlund-Venermo, M.; Hedman, K.; Ruuskanen, O.; Makela, M. New molecular virus detection methods and their clinical value in lower respiratory tract infections in children. *Paediatr. Respir. Rev.* **2013**, *14*, 38–45. [[CrossRef](#)] [[PubMed](#)]
14. Li, Y.; Yao, L.; Li, J.; Chen, L.; Song, Y.; Cai, Z.; Yang, C. Stability issues of RT-PCR testing of SAS-CoV-2 for hospitalized patients clinically diagnosed with COVID-19. *J. Med. Virol.* **2020**, *92*, 903–908. [[CrossRef](#)] [[PubMed](#)]
15. Notomi, T.; Mori, Y.; Tomita, N.; Kanda, H. Loop-mediated isothermal amplification (LAMP): Principle, features and future prospects. *J. Microbiol.* **2015**, *53*, 1–5. [[CrossRef](#)]
16. Vemula, S.V.; Zhao, J.; Liu, J.; Wang, X.; Biswas, S.; Hewlett, I. Current Approaches for Diagnosis of Influenza Virus Infections in Humans. *Viruses* **2016**, *8*, 96. [[CrossRef](#)]
17. Adams, E.; Ainsworth, M.; Anand, R.; Andersson, M.I.; Auckland, K.; Baillie, J.K.; Barnes, E.; Beer, S.; Bell, J.; Berry, T.; et al. Antibody testing for COVID-19: A report from the national covid scientific advisory panel. *Wellcome Open Res.* **2020**, *5*, 139. [[CrossRef](#)]
18. Gan, S.D.; Patel, K.R. Enzyme immunoassay and enzyme-linked immunosorbent assay. *J. Investig. Dermatol.* **2013**, *133*, 12. [[CrossRef](#)]
19. Nguyen, T.; Bang, D.D.; Wolff, A. 2019 novel coronavirus disease (covid-19): Paving the road for rapid detection and point-of-care diagnostics. *Micromachines* **2020**, *11*, 306. [[CrossRef](#)]
20. Visseaux, B.; le Hingrat, Q.; Collin, G.; Bouzid, D.; Lebourgeois, S.; le Pluart, D.; Deconinck, L.; Lescure, F.X.; Lucet, J.C.; Bouadma, L.; et al. Evaluation of the qiastat-dx respiratory SARS-CoV-2 panel, the first rapid multiplex PCR commercial assay for SARS-CoV-2 detection. *J. Clin. Microbiol.* **2020**, *58*, e00630-20. [[CrossRef](#)]
21. Souf, S. Recent advances in diagnostic testing for viral infections. *Biosci. Horiz. Int. J. Stud. Res.* **2016**, *9*, hzw010.
22. Soares, M.S.; Durigon, E.L.; Bersano, J.G.; Richtzenhain, L.J. Detection of porcine parvovirus DNA by the polymerase chain reaction assay using primers to the highly conserved nonstructural protein gene, NS-1. *J. Virol. Methods* **1999**, *78*, 191–198. [[CrossRef](#)] [[PubMed](#)]
23. Chalklen, T.; Jing, Q.; Kar-Narayan, S. Biosensors Based on Mechanical and Electrical Detection Techniques. *Sensors* **2020**, *20*, 5605. [[CrossRef](#)] [[PubMed](#)]
24. Xu, W.; Xie, L.; Ying, Y. Mechanisms and applications of terahertz metamaterial sensing: A review. *Nanoscale* **2017**, *9*, 13864–13878. [[CrossRef](#)]
25. Mauriz, E. Recent Progress in Plasmonic Biosensing Schemes for Virus Detection. *Sensors* **2020**, *20*, 4745. [[CrossRef](#)]
26. Yesilkoy, F.; Terborg, R.A.; Pello, J.; Belushkin, A.A.; Jahani, Y.; Pruneri, V.; Altug, H. Phase-sensitive plasmonic biosensor using a portable and large field-of-view interferometric microarray imager. *Light Sci. Appl.* **2018**, *7*, 17152. [[CrossRef](#)]
27. Ji, T.; Liu, Z.; Wang, G.; Guo, X.; Lai, C.; Chen, H.; Huang, S.; Xia, S.; Chen, B.; Jia, H.; et al. Detection of COVID-19: A review of the current literature and future perspectives. *Biosens. Bioelectron.* **2020**, *166*, 112455. [[CrossRef](#)]
28. Miller, B.S.; Bezing, L.; Gliddon, H.D.; Huang, D.; Dold, G.; Gray, E.R.; Heaney, J.; Dobson, P.J.; Nastouli, E.; Morton, J.J.; et al. Spin-enhanced nanodiamond biosensing for ultrasensitive diagnostics. *Nature* **2020**, *587*, 588–593. [[CrossRef](#)]
29. Moon, G.; Choi, J.r.; Lee, C.; Oh, Y.; Kim, K.; Kim, D. Machine learning-based design of meta-plasmonic biosensors with negative index metamaterials. *Biosens. Bioelectron.* **2020**, *164*, 112335. [[CrossRef](#)]
30. Maalouf, R.; Fournier-Wirth, C.; Coste, J.; Chebib, H.; Saikali, Y.; Vittori, O.; Errachid, A.; Cloarec, J.P.; Martelet, C.; Jaffrezic-Renault, N. Label-free detection of bacteria by electrochemical impedance spectroscopy: Comparison to surface plasmon resonance. *Anal. Chem.* **2007**, *79*, 4879–4886. [[CrossRef](#)]
31. Guner, H.; Ozgur, E.; Kokturk, G.; Celik, M.; Esen, E.; Topal, E.A.; Ayas, S.; Uludag, Y.; Elbuken, C.; Dana, A. A smartphone-based surface plasmon resonance imaging (SPRI) platform for on-site biodetection. *Sens. Actuators B Chem.* **2017**, *239*, 571–577. [[CrossRef](#)]
32. Al Ahmad, M.; Mustafa, F.; Ali, L.M.; Karakkat, J.V.; Rizvi, T.A. Label-Free Capacitance-Based Identification of Viruses. *Sci. Rep.* **2015**, *5*, 9809. [[CrossRef](#)] [[PubMed](#)]

33. Cossetini, A.; Selmi, L. On the Response of Nanoelectrode Impedance Spectroscopy Measures to Plant, Animal, and Human Viruses. *IEEE Trans. Nanobiosci.* **2018**, *17*, 102–109. [[CrossRef](#)] [[PubMed](#)]
34. MacCuspie, R.I.; Nuraje, N.; Lee, S.-Y.; Runge, A.; Matsui, H. Comparison of Electrical Properties of Viruses Studied by AC Capacitance Scanning Probe Microscopy. *J. Am. Chem. Soc.* **2008**, *130*, 887–891. [[CrossRef](#)] [[PubMed](#)]
35. Siegel, P. Terahertz technology in biology and medicine. *IEEE Trans. Microw. Theory* **2004**, *52*, 2438–2447. [[CrossRef](#)]
36. Zhang, X. Terahertz wave imaging: Horizons and hurdles. *Phys. Med. Biol.* **2002**, *47*, 3667–3677. [[CrossRef](#)]
37. Wallace, V.P.; Taday, P.F.; Fitzgerald, A.J.; Woodward, R.M.; Cluff, J.; Pye, R.J.; Arnone, D.D. Terahertz pulsed imaging and spectroscopy for biomedical and pharmaceutical applications. *Faraday Discuss.* **2004**, *126*, 55–263. [[CrossRef](#)]
38. Curcio, A.; Petrarca, M. Diagnosing plasmas with wideband terahertz pulses. *Opt. Lett.* **2019**, *44*, 1011–1014. [[CrossRef](#)]
39. Cheon, H.; Yang, J.-H.; Son, H.J. Toward clinical cancer imaging using terahertz spectroscopy. *IEEE J. Sel. Top. Quantum Electron.* **2017**, *23*, 8600109. [[CrossRef](#)]
40. Curcio, A.; Mou, S.; Palumbo, L.; Lupi, S.; Petrarca, M. Selection rules for the orbital angular momentum of optically produced THz radiation. *Opt. Lett.* **2021**, *46*, 1514–1517. [[CrossRef](#)]
41. Mou, S.; D’Arco, A.; Tomarchio, L.; Di Fabrizio, M.; Curcio, A.; Lupi, S.; Petrarca, M. Simultaneous elliptically and radially polarized THz from one-color laser-induced plasma filament. *New J. Phys.* **2021**, *23*, 063048. [[CrossRef](#)]
42. D’Arco, A.; Tomarchio, L.; Dolci, V.; Di Pietro, P.; Perucchi, A.; Mou, S.; Petrarca, M.; Lupi, S. Broadband anisotropic optical properties of the terahertz generator HMQ-TMS organic crystal. *Condens. Matter* **2020**, *5*, 47. [[CrossRef](#)]
43. Lupi, S.; Molle, A. Emerging Dirac materials for THz plasmonics. *Appl. Mater. Today* **2020**, *20*, 100732. [[CrossRef](#)]
44. Di Pietro, P.; Ortolani, M.; Limaj, O.; Di Gaspare, A.; Giliberti, V.; Giorgianni, F.; Brahlek, M.; Bansal, N.; Koirala, N.; Oh, S.; et al. Observation of dirac plasmons in a topological insulator. *Nat. Nanotechnol.* **2013**, *8*, 556–560. [[CrossRef](#)]
45. Galstyan, V.; D’Arco, A.; Di Fabrizio, M.; Poli, N.; Lupi, S.; Comini, E. Detection of volatile organic compounds: From chemical gas sensors to terahertz spectroscopy. *Rev. Anal. Chem.* **2021**, *40*, 33–57. [[CrossRef](#)]
46. D’Arco, A.; Di Fabrizio, M.; Dolci, V.; Marcelli, A.; Petrarca, M.; Della Ventura, G.; Lupi, S. Characterization of volatile organic compounds (VOCs) in their liquid-phase by terahertz time-domain spectroscopy. *Biomed. Opt. Exp.* **2019**, *11*, 1–7. [[CrossRef](#)]
47. Naftaly, M.; Vieweg, N.; Deninger, A. Industrial applications of terahertz sensing: State of play. *Sensors* **2019**, *19*, 4203. [[CrossRef](#)]
48. D’Arco, A.; Rocco, D.; Magboo, F.P.; Moffa, C.; Della Ventura, G.; Marcelli, A.; Palumbo, L.; Mattiello, L.; Lupi, S.; Petrarca, M. Terahertz continuous wave spectroscopy: A portable advanced method for atmospheric gas sensing. *Opt. Exp.* **2022**, *30*, 19005–19016. [[CrossRef](#)]
49. Smith, R.; Arnold, M. Selectivity of terahertz gas-phase spectroscopy. *Anal. Chem.* **2015**, *87*, 10679–10683. [[CrossRef](#)]
50. Rothbart, N.; Holz, O.; Koczulla, R.; Schmalz, K.; Hübers, H. Analysis of human breath by millimeter-wave/terahertz spectroscopy. *Sensors* **2019**, *19*, 12719. [[CrossRef](#)]
51. Macis, S.; Paolozzi, M.C.; D’Arco, A.; Tomarchio, L.; Di Gaspare, A.; Lupi, S. Terahertz Resonators Based on YBa<sub>2</sub>Cu<sub>3</sub>O<sub>7</sub> High-Tc Superconductor. *Appl. Sci.* **2022**, *12*, 10242. [[CrossRef](#)]
52. Tomarchio, L.; Macis, S.; D’Arco, A.; Mou, S.; Grilli, A.; Romani, M.; Cestelli Guidi, M.; Hu, K.; Kukunuri, S.; Jeong, S.; et al. Disordered photonics behavior from terahertz to ultraviolet of a three-dimensional graphene network. *NPG Asia Mater.* **2021**, *13*, 73. [[CrossRef](#)]
53. Rau, J.V.; Fadeeva, I.V.; Forysenkova, A.A.; Davydova, G.A.; Fosca, M.; Filippov, Y.Y.; Antoniac, I.V.; Antoniac, A.; D’Arco, A.; Di Fabrizio, M.; et al. Strontium substituted tricalcium phosphate bone cement: Short and long-term time-resolved studies and in vitro properties. *Adv. Mater. Interfaces* **2022**, *9*, 2200803. [[CrossRef](#)]
54. Grazianetti, C.; Bonaventura, E.; Martella, C.; Molle, A.; Lupi, S. Optical Properties of Stanene-like Nanosheets on Al<sub>2</sub>O<sub>3</sub>: Implications for Xene Photonics. *ACS Appl. Nano Mater.* **2021**, *4*, 2351–2356. [[CrossRef](#)] [[PubMed](#)]
55. D’Arco, A.; Mussi, V.; Petrov, S.; Tofani, S.; Petrarca, M.; Beccherelli, R.; Dimitrov, D.; Marinova, V.; Lupi, S.; Zografopoulos, D. Fabrication and spectroscopic characterization of graphene transparent electrodes on flexible cyclo-olefin substrates for terahertz electro-optic applications. *Nanotechnology* **2020**, *31*, 364006. [[CrossRef](#)]
56. Federici, J.; Schulkin, B.; Huang, F.; Gary, D.; Barat, R.; Oliveira, F.; Zimdars, D. THz imaging and sensing for security applications—explosives, weapons and drugs. *Semicond. Sci. Technol.* **2005**, *20*, 266. [[CrossRef](#)]
57. Wang, K.; Sun, D.W.; Pu, H. Emerging non-destructive terahertz spectroscopic imaging technique: Principle and applications in the agri-food industry. *Trend Food Sci. Technol.* **2017**, *67*, 93–105. [[CrossRef](#)]
58. Cosentino, A. Terahertz and cultural heritage science: Examination of art and archeology. *Technologies* **2016**, *4*, 6. [[CrossRef](#)]
59. D’Arco, A.; Di Fabrizio, M.; Dolci, V.; Petrarca, M.; Lupi, S. THz pulsed imaging in biomedical applications. *Condens. Matter* **2020**, *5*, 25. [[CrossRef](#)]
60. Di Fabrizio, M.; D’Arco, A.; Mou, S.; Palumbo, L.; Petrarca, M.; Lupi, S. Performance evaluation of a THz pulsed imaging system: Point spread function, broadband THz beam visualization and image reconstruction. *Appl. Sci.* **2021**, *11*, 562. [[CrossRef](#)]
61. Mancini, T.; Mosetti, R.; Marcelli, A.; Petrarca, M.; Lupi, S.; D’Arco, A. Terahertz spectroscopic analysis in protein dynamics: Current status. *Radiation* **2022**, *2*, 100–123. [[CrossRef](#)]
62. Di Fabrizio, M.; Lupi, S.; D’Arco, A. Virus recognition with terahertz radiation: Drawbacks and potentialities. *J. Phys. Photonics* **2021**, *3*, 032001. [[CrossRef](#)]

63. Fardelli, E.; D'Arco, A.; Lupi, S.; Billi, D.; Moeller, R.; Cestelli Guidi, M. Spectroscopic evidence of the radioresistance of Chroococciopsis biosignatures: A combined Raman, FT-IR and THz-TDs spectroscopy study. *Spectrochim. Acta Part A Mol. Biomol. Spectrosc.* **2023**, *288*, 122148. [[CrossRef](#)] [[PubMed](#)]
64. Manti, L.; D'Arco, A. Cooperative biological effects between ionizing radiation and other physical and chemical agents. *Mutat. Res. Rev. Mutat. Res.* **2010**, *704*, 115–122. [[CrossRef](#)] [[PubMed](#)]
65. Parrott, E.P.J.; Zeitler, J.A. Terahertz Time-Domain and Low-Frequency Raman Spectroscopy of Organic Materials. *Appl. Spectrosc.* **2015**, *69*, 1–25. [[CrossRef](#)]
66. Walther, M.; Plochocka, P.; Fischer, B.; Helm, H.; Jepsen, P. Collective vibrational modes in biological molecules investigated by terahertz time-domain spectroscopy. *Biopolymers* **2002**, *67*, 310–313. [[CrossRef](#)]
67. Lee, D.; Cheon, H.; Jeong, S.-Y.; Son, J.-H. Transformation of terahertz vibrational modes of cytosine under hydration. *Sci Rep* **2020**, *10*, 10271. [[CrossRef](#)]
68. Ghann, W.; Uddin, L. Terahertz (THz) spectroscopy: A cutting-edge technology terahertz spectroscopy—A cutting edge. In *Terahertz (THz) Spectroscopy: A Cutting Edge Technology Terahertz Spectroscopy—A Cutting Edge*; Uddin, J., Ed.; Chapman and Hall, IntechOpen Limited: London, UK, 2017.
69. Yang, X.; Zhao, X.; Yang, K.; Liu, Y.; Liu, Y.; Fu, W.; Luo, Y. Biomedical applications of terahertz spectroscopy and imaging. *Trends Biotechnol.* **2016**, *34*, 810–824. [[CrossRef](#)]
70. Rezvani, S.J.; Di Gioacchino, D.; Tofani, S.; D'Arco, A.; Ligi, C.; Lupi, S.; Gatti, C.; Cestelli Guidi, M.; Marcelli, A. A cryogenic magneto-optical device for long wavelength radiation. *Rev. Sci. Instrum.* **2020**, *91*, 075103. [[CrossRef](#)]
71. Fedulova, E.; Nazarov, M.; Angeluts, A.; Kitai, M.; Sokolov, V.; Shkurinov, A. Studying of dielectric properties of polymers in the terahertz frequency range. In *Optical Technologies in Biophysics and Medicine XIII, Proceedings of the Saratov Fall Meeting 2011, Saratov, Russia, 27–30 September 2011*; SPIE: Bellingham, WA, USA, 2011.
72. Marcelli, A.; Irizawa, A.; Lupi, S. THz: Research frontiers for new sources, imaging and other advanced technologies. *Condens. Matter* **2019**, *6*, 23.
73. Lin, H.; Withayachumnankul, W.; Fischer, B.; Mickan, S.; Abbott, D. Gas recognition with terahertz time-domain spectroscopy and spectral catalog: A preliminary study. *Terahertz Photonics* **2008**, *6840*, 68400X.
74. Zhang, X.-C.; Jingzhou, X. *Introduction to THz Wave Photonics*, 1st ed.; Springer: Boston, MA, USA, 2010.
75. Burford, N.; El-Shenawee, M.O. Review of terahertz photoconductive antenna technology. *Opt. Eng.* **2017**, *56*, 010901. [[CrossRef](#)]
76. Dexheimer, S.L. *Terahertz Spectroscopy: Principles and Applications*; CRC Press: Boca Raton, FL, USA, 2017.
77. Naftaly, M. *Terahertz Metrology*; Artech House: London, UK, 2015.
78. Seo, M.; Park, H.-R. Terahertz Biochemical Molecules-specific sensors. *Adv. Opt. Mater.* **2019**, *8*, 1900662. [[CrossRef](#)]
79. Ajito, K.; Ueno, Y. THz chemical imaging for biological applications. *IEEE Trans. Terahertz Sci. Technol.* **2011**, *1*, 293–300. [[CrossRef](#)]
80. Cooksey, C.C.; Greer, B.J.; Heilweil, E.J. Terahertz Spectroscopy of L-Proline in Reverse Aqueous Micelles. *Chem. Phys. Lett.* **2009**, *467*, 424–429. [[CrossRef](#)]
81. Abbe, E. Beitrage zur theorie des mikroskops und der mikroskopischen wahrnehmung. *Archiv. Mikrosk. Anat.* **1873**, *9*, 413–468. [[CrossRef](#)]
82. Park, S.J.; Cha, S.H.; Shin, G.A.; Ahn, Y.H. Sensing viruses using terahertz nano-gap metamaterials. *Biomed. Opt. Express* **2017**, *8*, 3551–3558. [[CrossRef](#)]
83. Lee, D.-K.; Kang, J.-H.; Know, J.; Lee, J.-S.; Lee, S.; Woo, D.; Kim, J.; Song, C.-S.; Park, Q.; Seo, M. Nano metamaterials for ultrasensitive terahertz biosensing. *Sci. Rep.* **2017**, *7*, 8146. [[CrossRef](#)]
84. Sun, Y.; Zhang, Y.; Pickwell-MacPherson, E. Investigating antibody interactions with a polar liquid using terahertz pulsed spectroscopy. *Biophys. J.* **2011**, *100*, 225–231. [[CrossRef](#)]
85. Zhou, R.; Wang, C.; Wendao, X.; Xie, L. Biological applications of terahertz technology based on nanomaterials and nanostructures. *Nanoscale* **2019**, *11*, 3445–3457. [[CrossRef](#)]
86. Sun, Y.; Zhong, J.; Zhang, C.; Zuo, J.; Pickwell-MacPherson, E. Label-free detection and characterization of the binding of hemagglutinin protein and broadly neutralizing monoclonal antibodies using terahertz spectroscopy. *J. Biomed. Opt.* **2015**, *20*, 037006. [[CrossRef](#)]
87. Zhou, R.; Wang, C.; Huang, Y.; Huang, K.; Wang, Y.; Xu, W.; Xie, L.; Ying, Y. Label-free Terahertz Microfluidic Biosensor for Sensitive DNA Detection Using Graphene-Metasurface Hybrid Structures. *Biosens. Bioelectron.* **2021**, *188*, 113336. [[CrossRef](#)]
88. Tang, Q.; Liang, M.; Yi, L.; Wong, P.K.; Wilmink, G.J.; Zhang, D.D.; Xin, H. Microfluidic devices for terahertz spectroscopy of live cells toward lab-on-a-chip applications. *Sensors* **2016**, *16*, 476. [[CrossRef](#)]
89. Chen, X.; Fan, W. Ultrasensitive terahertz metamaterial sensor based on spoof surface plasmon. *Sci. Rep.* **2017**, *7*, 2092. [[CrossRef](#)]
90. Samy Saadeldin, A.; Hameed, M.F.O.; Elkaramany, E.M.A.; Obayya, S.S.A. Highly sensitive terahertz metamaterial sensor. *IEEE Sens. J.* **2019**, *19*, 7993–7999. [[CrossRef](#)]
91. Nickpay, M.R.; Danaie, M.; Shahzadi, A. Highly Sensitive THz Refractive Index Sensor Based on Folded Split-Ring Metamaterial Graphene Resonators. *Plasmonics* **2022**, *17*, 237–248. [[CrossRef](#)]
92. Karthikeyan, M.; Jayabala, P.; Ramachandran, S.; Dhanabalan, S.S.; Sivanesan, T.; Ponnusamy, M. Tunable Optimal Dual Band Metamaterial Absorber for High Sensitivity THz Refractive Index Sensing. *Nanomaterials* **2022**, *12*, 2693. [[CrossRef](#)]
93. Cui, Z.; Wang, Y.; Shi, Y.; Zhu, Y.; Zhang, D.; Hong, Z.; Feng, X. Significant sensing performance of an all-silicon terahertz metasurface chip for Bacillus thuringiensis Cry1Ac protein. *Photonics Res.* **2022**, *10*, 740–746. [[CrossRef](#)]

94. Nickpay, M.R.; Danaie, M.; Shahzadi, A. Graphene-based metamaterial absorber for refractive index sensing applications in terahertz band. *Diam. Relat. Mater.* **2022**, *130*, 109539. [[CrossRef](#)]
95. Geng, Z.; Zhang, X.; Fan, Z.; Lv, X.; Chen, H. A Route to Terahertz Metamaterial Biosensor Integrated with Microfluidics for Liver Cancer Biomarker Testing in Early Stage. *Sci. Rep.* **2017**, *7*, 16378–16411. [[CrossRef](#)]
96. Bhardwaj, S.K.; Bhardwaj, N.; Kumar, V.; Bhatt, D.; Azzouz, A.; Bhaumik, J.; Kim, K.-H.; Deep, A. Recent progress in nanomaterial-based sensing of airborne viral and bacterial pathogens. *Environ. Int.* **2021**, *146*, 106183. [[CrossRef](#)]
97. Yang, Y.; Xu, D.; Zhang, W. High-sensitivity and Label-free Identification of a Transgenic Genome Using a Terahertz Meta-Biosensor. *Opt. Express* **2018**, *26*, 31589–31598. [[CrossRef](#)]
98. Zhou, J.; Zhao, X.; Huang, G.; Yang, X.; Zhang, Y.; Zhan, X.; Tian, H.; Xiong, Y.; Wang, Y.; Fu, W. Molecule-Specific Terahertz Biosensors Based on an Aptamer Hydrogel-Functionalized Metamaterial for Sensitive Assays in Aqueous Environments. *ACS Sens.* **2021**, *6*, 1884–1890. [[CrossRef](#)]
99. Zhang, Y.; Han, Z. Spoof surface plasmon based planar antennas for the realization of terahertz hotspots. *Sci. Rep.* **2015**, *5*, 18606. [[CrossRef](#)]
100. Cheng, D.; Xia, H.; Huang, X.; Zhang, B.; Liu, G.; Shu, G.; Fang, C.; Wang, J.; Luo, Y. Terahertz biosensing metamaterial absorber for virus detection based on spoof surface plasmon polaritons. *Int. J. RF Microw. Computer-Aided Eng.* **2018**, *28*, e21448. [[CrossRef](#)]
101. Chen, X.; Park, H.-R.; Pelton, M.; Piao, X.; Lindquist, N.C.; Im, H.; Kim, Y.J.; Ahn, J.S.; Ahn, K.J.; Park, N.; et al. Atomic layer lithography of wafer-scale nanogap arrays for extreme confinement of electromagnetic waves. *Nat. Commun.* **2013**, *4*, 2361. [[CrossRef](#)]
102. Tang, W.X.; Zhang, H.C.; Ma, H.F.; Jiang, W.X.; Cui, T.J. Concept, theory, design and applications of spoof surface plasmon polaritons at microwave frequencies. *Adv. Opt. Mater.* **2019**, *7*, 1800421. [[CrossRef](#)]
103. O'Hara, J.F.; Singh, R.; Brener, I.; Smirnova, E.; Han, J.; Taylor, A.J.; Zhang, W. Thin-Film Sensing with Planar Terahertz Metamaterials: Sensitivity and Limitations. *Opt. Express* **2008**, *16*, 1786–1795. [[CrossRef](#)]
104. Tao, H.; Strikwerda, A.C.; Liu, M.; Mondia, J.P.; Ekmekci, E.; Fan, K.; Kaplan, D.L.; Padilla, W.J.; Zhang, X.; Averitt, R.D.; et al. Performance Enhancement of Terahertz Metamaterials on Ultrathin Substrates for Sensing Applications. *Appl. Phys. Lett.* **2010**, *97*, 261909. [[CrossRef](#)]
105. Tao, H.; Chieffo, L.R.; Brenckle, M.A.; Siebert, S.M.; Liu, M.; Strikwerda, A.C.; Fan, K.; Kaplan, D.L.; Zhang, X.; Averitt, R.D.; et al. Metamaterials on Paper as a Sensing Platform. *Adv. Mater.* **2011**, *23*, 3197–3201. [[CrossRef](#)]
106. Limaj, O.; Nucara, A.; Lupi, S.; Ortolani, M.; Di Gaspare, A.; Palange, E.; Carelli, P. Scaling the spectral response of metamaterial dipolar filters in the terahertz. *Opt. Commun.* **2011**, *284*, 1690–1693. [[CrossRef](#)]
107. D'Apuzzo, F.; Candeloro, P.; Domenici, F.; Autore, M.; Di Pietro, P.; Perucchi, A.; Roy, P.; Sennato, S.; Bordi, F.; Di Fabrizio, E.M.; et al. Resonating terahertz response of periodic arrays of subwavelength apertures. *Plasmonics* **2015**, *10*, 45–50. [[CrossRef](#)]
108. D'Apuzzo, F.; Piacenti, A.R.; Giorgianni, F.; Autore, M.; Cestelli Guidi, M.A.; Marcelli, A.; Schade, U.; Ito, Y.; Chen, M.; Lupi, S. Terahertz and mid-infrared plasmons in three-dimensional nanoporous graphene. *Nat. Commun.* **2017**, *8*, 14885. [[CrossRef](#)]
109. Hong, J.T.; Jun, S.W.; Cha, S.H.; Park, J.Y.; Lee, S.; Shin, G.A.; Ahn, Y.H. Enhanced sensitivity in THz plasmonic sensors with silver nanowires. *Sci. Rep.* **2018**, *8*, 15536. [[CrossRef](#)]
110. Terracciano, M.; Rea, I.; Politi, J.; De Stefano, L. Optical characterization of aminosilane-modified silicon dioxide surface for biosensing. *J. Eur. Opt. Soc.-Rap.* **2013**, *8*, 13075. [[CrossRef](#)]
111. De Stefano, L.; Oliviero, G.; Amato, J.; Borbone, N.; Piccialli, G.; Mayol, L.; Rendina, I.; Terracciano, M.; Rea, I. Aminosilane functionalizations of mesoporous oxidized silicon for oligonucleotide synthesis and detection. *J. R. Soc. Interface* **2013**, *10*, 20130160. [[CrossRef](#)]
112. Terracciano, M.; Galstyan, V.; Rea, I.; Casalino, M.; De Stefano, L.; Sberveglieri, G. Chemical modification of TiO<sub>2</sub> nanotube arrays for label-free optical biosensing applications. *Appl. Surf. Sci.* **2017**, *419*, 235–240. [[CrossRef](#)]
113. Xiaojun, W.; Quan, B.; Pan, X.; Xinlong, X.; Xinchao, L.; Changzhi, G.; Wang, L. Alkanethiol-functionalized terahertz metamaterial as label-free, highly-sensitive and specific biosensor. *Biosens. Bioelectron.* **2013**, *42*, 626–631.
114. Li, Y.; Wang, X.; Liu, Y.; Jin, W.; Tian, H.; Xie, F.; Xia, K.; Zhang, X.; Fu, W.; Zhang, Y. Flexible Terahertz Metamaterial Biosensor for Ultra-Sensitive Detection of Hepatitis B Viral DNA Based on the Metal-Enhanced Sandwich Assay. *Front. Bioeng. Biotechnol.* **2022**, *10*, 930800. [[CrossRef](#)]
115. Keshavarz, A.; Vafapour, Z. Sensing Avian influenza viruses using terahertz metamaterial reflector. *IEEE Sens. J.* **2019**, *19*, 5161–5166. [[CrossRef](#)]
116. Cheng, R.; Xu, L.; Yu, X.; Zou, L.; Shen, Y.; Deng, X. High-sensitivity biosensor for identification of protein based on terahertz Fano resonance metasurfaces. *Opt. Commun.* **2020**, *473*, 125850. [[CrossRef](#)]
117. Amin, M.; Siddiqui, O.; Farhat, M. Linear and Circular Dichroism in Graphene-Based Reflectors for Polarization Control. *Phys. Rev. Applied* **2020**, *13*, 024046. [[CrossRef](#)]
118. Amin, M.; Siddiqui, O.; Abutarboush, A.; Farhat, M.; Ramzan, R. A THz graphene metasurface for polarization selective virus sensing. *Carbon* **2021**, *176*, 580–591. [[CrossRef](#)] [[PubMed](#)]
119. Ahmadivand, A.; Gerislioglu, B.; Tomitaka, A.; Manickam, P.; Kaushik, A.; Bhansali, S.; Nair, M.; Pala, N. Extreme sensitive metasensor for targeted biomarkers identification using colloidal nanoparticles-integrated plasmonic unit cells. *Biomed. Opt. Express* **2018**, *9*, 373–386. [[CrossRef](#)] [[PubMed](#)]

120. Ahmadivand, A.; Gerislioglu, B.; Manickam, P.; Kaushik, A.; Bhansali, S.; Nair, M.; Pala, N. Rapid Detection of Infectious Envelope Proteins by Magnetoplasmonic Toroidal Metasensors. *ACS Sens.* **2017**, *2*, 1359–1368. [[CrossRef](#)]
121. Ahmadivand, A.; Gerislioglu, B.; Ahuja, R.; Mishra, Y.K. Terahertz plasmonics: The rise of toroidal metadevices towards immunobiosensings. *Mater. Today* **2020**, *32*, 108–130. [[CrossRef](#)]
122. Jin, C.; Wu, Z.; Molinski, J.H.; Zhou, J.; Ren, Y.; Zhang, J.X.J. Plasmonic nanosensors for point-of-care biomarker detection. *Mat. Today Bio* **2022**, *14*, 100263. [[CrossRef](#)]
123. Ahmadivand, A.; Gerislioglu, B.; Ramezani, Z.; Ghoreishi, S.A. Attomolar detection of low-molecular weight antibiotics using midinfrared-resonant toroidal plasmonic metachip technology. *Phys. Rev. Appl.* **2019**, *12*, 034018. [[CrossRef](#)]
124. Ahmadivand, A.; Gerislioglu, B.; Ramezani, Z.; Kaushik, A.; Manickam, P.; Ghoreish, S.A. Functionalized terahertz plasmonic metasensors: Femtomolar-level detection of SARS-CoV-2 spike proteins. *Biosens. Bioelectron.* **2021**, *177*, 112971. [[CrossRef](#)]
125. Shi, W.; Fan, F.; Li, S.; Zhang, Z.; Liu, H.; Wang, X.; Chang, S. Terahertz immunosensing assisted by functionalized Au NPs based on all-dielectric metasurface. *Sens. Actuators B. Chem.* **2022**, *362*, 131777. [[CrossRef](#)]
126. Niu, Q.; Zhang, R.; Yang, Y. High Sensitivity and Label-Free Detection of the SARS-CoV-2 S1 Protein Using a Terahertz Meta-Biosensor. *Front. Phys.* **2022**, *10*, 859924. [[CrossRef](#)]
127. Biswas, S.; Adhikari, S.; Chawla, R.; Maiti, N.; Bhatia, D.; Phukan, P.; Mukherjee, M. Artificial intelligence enabled non-invasive T-ray imaging technique for early detection of coronavirus infected patients. *Inform. Med. Unlocked* **2022**, *32*, 101025. [[CrossRef](#)] [[PubMed](#)]
128. Wu, J.; Yuan, T.; Liu, J.; Qin, J.; Hong, Z.; Li, J.; Du, Y. Terahertz Metamaterial Sensor with Ultra-High Sensitivity and Tunability Based on Photosensitive Semiconductor GaAs. *IEEE Sens. J.* **2022**, *22*, 15961–15966. [[CrossRef](#)]

**Disclaimer/Publisher's Note:** The statements, opinions and data contained in all publications are solely those of the individual author(s) and contributor(s) and not of MDPI and/or the editor(s). MDPI and/or the editor(s) disclaim responsibility for any injury to people or property resulting from any ideas, methods, instructions or products referred to in the content.